On the Combination Reactions of Hydrogen Atoms with Resonance-Stabilized Hydrocarbon Radicals[†]

Lawrence B. Harding* and Stephen J. Klippenstein

Chemistry Division, Argonne National Laboratory, Argonne, Illinois 60439

Yuri Georgievskii

Combustion Research Facility, Sandia National Laboratories, Livermore, California 94551-0969

Procedures for accurately predicting the kinetics of H atom associations with resonance stabilized hydrocarbon radicals are described and applied to a series of reactions. The approach is based on direct CASPT2/cc-pvdz evaluations of the orientation dependent interaction energies within variable reaction coordinate transition state theory. One-dimensional corrections to the interaction energies are estimated from a CASPT2/aug-cc-pvdz minimum energy path (MEP) on the specific reaction of interest and a CASPT2/aug-cc-pvtz MEP for the H + CH$_3$ reaction. A dynamical correction factor of 0.9 is also applied. For the H + propargyl, allyl, cyclopentadienyl, and benzyl reactions, where the experimental values appear to be quite well determined, theory and experiment agree to within their error bars. Predictions are also made for the combinations with triplet propargylene, CH$_2$CCCH, CH$_3$CCCH$_2$, CH$_2$CHCCH$_2$, CH$_3$CHCCH, *cyclic*-C$_4$H$_5$, CH$_2$CCCCH, and CHCCHCCH.

1. Introduction

The chemistry of combustion is essentially the kinetics of radical reactions. Resonance-stabilized radicals (RSRs) are among the most prominent radicals in hydrocarbon flames due in large part to their enhanced thermodynamic stability. These radicals also have a lower reactivity than other radicals due to the presence of larger reactive barriers arising from the loss of the resonances during reaction.

One result of the prominence of RSRs is that they play a central role in the growth of higher hydrocarbons. For example, pioneering work by Miller[1−5] has led to the conclusion that the self-recombination of propargyl radicals is the dominant step in the formation of benzene for many hydrocarbon fuels.[6] This formation of the first aromatic ring is a key precursor to the formation of polycyclic aromatic hydrocarbons (PAHs), which, in turn, are key precursors to the formation of soot. The growth of larger PAHs may also involve the addition kinetics of RSRs.[7,8]

There is considerable current interest in the development of accurate models of the chemistry involved in PAH and soot formation.[9,10] The importance of RSRs in the hydrocarbon growth process implies that such models must include an accurate description of their kinetics. One particularly important class of reactions for the RSRs involves their combination kinetics with other radicals, particularly other RSRs. Unfortunately, due to the difficulty of producing and observing isolated radicals, there is very little experimental data regarding the kinetics of such reactions. Furthermore, the theoretical analysis of radical−radical reactions is complicated by the need to employ multireference ab initio methods and to include treat-

ments of anharmonic effects in the transition state region. Thus, there have also been only a few prior theoretical studies of such reactions.

We have recently described an ab initio transition state theory based procedure for accurately predicting the combination kinetics of two radicals.[11,12] This variable reaction coordinate transition state theory (VRC−TST)[13,14] based approach employs a direct evaluation of the orientation dependent interaction energies at the CASPT2[15,16] level. In our initial applications of this approach, we focused on the combination of simple hydrocarbon alkyl radicals first with H atoms[11] and then with other simple hydrocarbon alkyl radicals.[12] In this article, we extend this approach to the study of the combination of hydrocarbon RSRs with hydrogen atoms. In addition to providing kinetic estimates for the RSR + H reactions, this work will also serve as a useful precursor to subsequent studies of the combination kinetics of the RSRs with other simple alkyl radicals and with other RSRs.

The resonance-stabilized radicals ^{3}CHCCH (triplet propargylene), CH$_2$CCH (propargyl), CH$_2$CHCH$_2$ (allyl), CH$_2$CCCH (*i*-C$_4$H$_3$), CH$_2$CHCCH$_2$ (*i*-C$_4$H$_5$), CH$_3$CCCH$_2$, CH$_3$CHCCH, CH$_2$CCCCH (*i*-C$_5$H$_3$), CHCCHCCH (*n*-C$_5$H$_3$), and cyclopentadienyl have each been observed at significant concentrations in recent photoionization mass spectrometry studies of hydrocarbon flames.[17−20] Related observations, without the isomer identification, have been made in molecular beam mass spectrometry studies employing electron impact ionization.[10,21] For each of these RSRs, one can readily envision a route to the formation of the first aromatic ring involving a bimolecular reaction with some other prominent flame species.[6] Thus, in this article, we consider the H atom addition kinetics for each of them. For completeness, we also consider the *cyclic*-C$_4$H$_5$ radical, which has a similar thermodynamic stability to the other C$_4$H$_5$ RSRs.[18] The benzyl radical is another key RSR, being
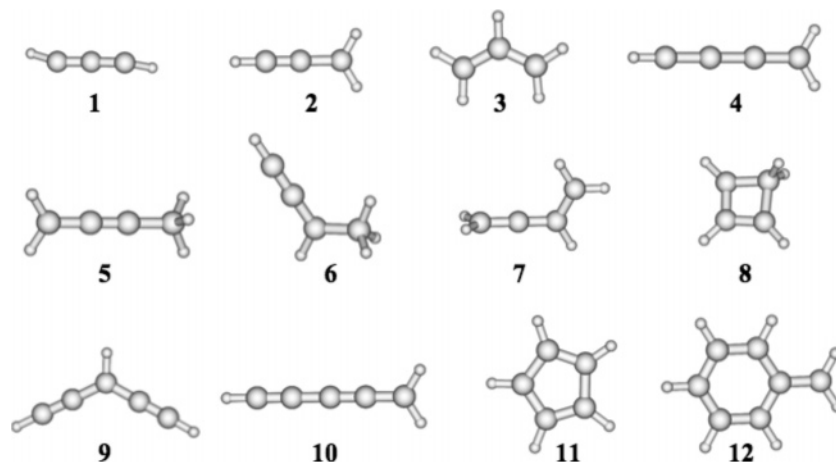
Figure 1. Structures of the 12 resonance-stabilized C_3, C_4, C_5, and C_7 hydrocarbon radicals considered here.

suggested to play an important role in subsequent ring formation and hydrocarbon growth through reactions such as benzyl plus propargyl recombination.[7] In a related study,[22] we have recently examined the combination kinetics of benzyl radical with H atoms, and we include a brief review of this study here. The geometrical structures of the complete set of radicals considered here are illustrated in Figure 1.

The methodology of the present direct CASPT2 VRC−TST calculations is summarized in Section 2. The presence of resonances in the electronic structure of these radicals necessitates the implementation of two modifications to the approach employed in our prior direct CASPT2 VRC−TST studies. In particular, a larger CAS space, consisting of all the π and π^* orbitals, is used. Also, we now incorporate system-specific basis set corrections for the potential along the minimum energy path. A more detailed discussion of these extensions is included in Section 2.

The results of the current calculations are presented and discussed in Section 3. For the C3 radicals, i.e., triplet propargylene, propargyl, and allyl, comparisons with related calculations and/or with experiment allow us to test the adequacy of various aspects of the analysis. For cyclopentadienyl and benzyl radicals, comparisons with experiment yield an indication of the accuracy of the approach. The results for the remaining systems allow us to examine various chemical aspects of the calculations such as the effect of steric hindrance on the rate coefficients.

2. Methods

2.1. Electronic Structure Methods. The electronic structure calculations reported here are of the CASPT2 variety. The CAS reference spaces are chosen to include the two radical orbitals and both π and π^* orbitals for each π bond in the hydrocarbon radical (both in-plane and out-of-plane π bonds). The reasons for including the additional π and π^* orbitals in the active space will be discussed in Section 3. The CASPT2 calculations employ the Dunning[23−25] correlation consistent basis sets, and the formalism of Celani and Werner[26] and were done using the MOLPRO program package.[27,28]

As discussed in the next section, the transition state theory method used here neglects changes in the internal degrees of freedom of the reactants, i.e., the geometries of the hydrocarbon radicals are kept fixed at their asymptotic, equilibrium geometries. With this approximation, all of the H + hydrocarbon radical association reactions can be treated using three-dimensional potential surfaces where the three dimensions
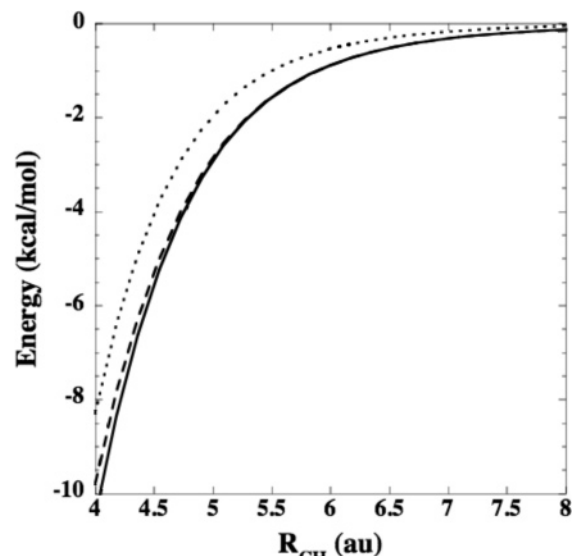
Figure 2. Potential curves for H + C_3H_2. The solid line corresponds to CASPT2/aug-cc-pvtz, the dashed line to CASPT2/aug-cc-pvdz, and the dotted line to CASPT2/cc-pvdz.

correspond to motions of the hydrogen atom relative to the rigid, fixed hydrocarbon radical. The kinetic predictions are only weakly dependent on the equilibrium geometries of these radicals, and so they were simply determined from B3LYP/6-31G* calculations using the GAUSSIAN98 program.[29]

In Figure 2, we compare one-dimensional, CASPT2, potential curves for H + C_3H_2 calculated using the cc-pvdz, aug-cc-pvdz, and aug-cc-pvtz basis sets. All curves are calculated with the same fixed orientation for the approach of the H atom to the C_3H_2 radical. This orientation is chosen to minimize the energy at a distance of 6 au. On the scale of this plot, calculations using an even larger aug-cc-pvqz basis set are indistinguishable from the aug-cc-pvtz calculations. In Figure 3, we plot the differences between the aug-cc-pvtz and aug-cc-pvdz curves in Figure 2, the differences between the aug-cc-pvdz and cc-pvdz curves from Figure 2, and the differences between aug-cc-pvtz and aug-cc-pvdz curves for H + CH_3. From these plots, it can be seen that the aug-cc-pvtz potential curve is in the range of 30−50% more attractive than the cc-pvdz curve in this kinetically sensitive, long-range region. A 40% difference in the attractiveness of these two potentials translates into an ∼40% difference in the room temperature association rate coefficients calculated using these two potentials (see below).

Reactions of H Atoms with Hydrocarbon Radicals

J. Phys. Chem. A, Vol. 111, No. 19, 2007 **3791**
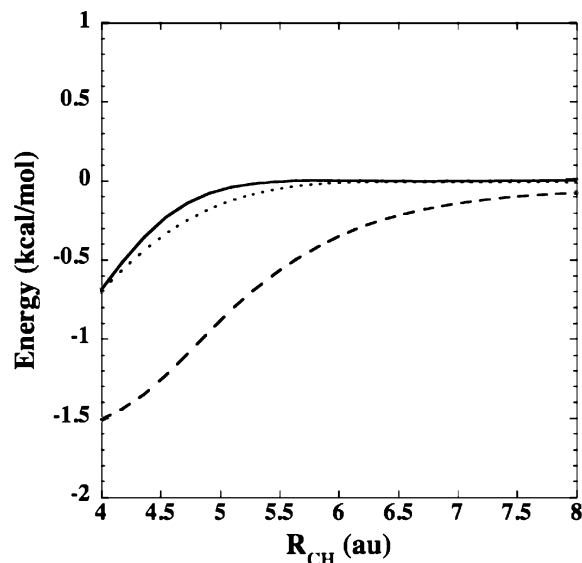
Figure 3. Difference potential curves. The solid line is $\Delta_{atz-adz} = V_{CASPT2/aug-cc-pvtz} - V_{CASPT2/aug-cc-pvdz}$ for H + C$_3$H$_2$, the dashed line is $\Delta_{adz-dz} = V_{CASPT2/aug-cc-pvdz} - V_{CASPT2/cc-pvdz}$ for H + C$_3$H$_2$, and the dotted line is $\Delta_{CH4} = V_{CASPT2/aug-cc-pvtz} - V_{CASPT2/aug-cc-pvdz}$ for H + CH$_3$.

To correct the cc-pvdz calculations for this basis set deficiency, we will make two key approximations. First, we assume that the difference potential shown in Figure 3, although calculated for one particular orientation is, to a reasonable approximation, independent of orientation. With this assumption then we can approximate a three-dimensional, aug-cc-pvdz potential as the sum of a three-dimensional cc-pvdz potential plus the one-dimensional difference potential (aug-cc-pvdz minus cc-pvdz) shown in Figure 3. The second approximation is designed to correct for the small residual difference between the aug-cc-pvdz potential and the more accurate aug-cc-pvtz potential. Here again we assume the difference is independent of orientation. We make the additional assumption that this difference is the same for all hydrocarbon radicals and use a difference potential, evaluated for H + CH$_3$ (also shown in Figure 3). With these two approximations, we then define the potential, V, for an H atom interacting with an arbitrary, rigid, hydrocarbon radical as follows,

$$V(R,\theta,\phi) = V_{CASPT2/cc-pvdz}(R,\theta,\phi) + \Delta_{adz-dz}(R) + \Delta_{CH4}(R) \quad (10)$$

where $V_{CASPT2/cc-pvdz}(R,\theta,\phi)$ is the three-dimensional CASPT2/cc-pvdz potential for an H atom interacting with the hydrocarbon radical, R is the distance between the H atom and the closest radical carbon atom, θ and ϕ are the two orientational degrees of freedom, Δ_{adz-dz} is the difference between the CASPT2/aug-cc-pvdz and CASPT2/cc-pvdz potentials for H + the radical for a fixed orientation, as shown in Figure 3 for H + C$_3$H$_2$, and Δ_{CH4} is the difference between the CASPT2/aug-cc-pvtz and CASPT2/aug-cc-pvdz potentials for H + CH$_3$ calculated along the C$_3$ axis of CH$_3$. The justification for this definition will be given in Sections 3.1.1–3.1.4, where we will compare potentials defined by eq 10 and potentials derived directly from CASPT2/aug-cc-pvtz calculations.

For the more highly unsaturated radicals, the possibility exists for an addition on triplet surfaces forming triplet carbenes. This possibility was checked for CH$_2$CCCH and CH$_2$CCCCH. In both cases, exothermic triplet channels were found to exist, but these channels are predicted to have small barriers (1–5 kcal/mol).

In these channels, the H atom attacks a π bond in a plane perpendicular to that of the radical orbital. These triplet channels then are analogous to H atom additions to closed shell, unsaturated hydrocarbons such as acetylene or ethylene. Such processes are known to have small barriers[30–32] with correspondingly small rates, except, perhaps, at quite high temperatures. It was assumed that any other triplet channels that exist would also have barriers and therefore would not be competitive with the barrierless reactions on the singlet surface.

2.2. Transition State Theory Methods. The direct CASPT2 variable reaction coordinate (VRC) transition state theory (TST) approach was summarized in some detail in our recent invited articles.[11,12] Thus, we provide here only a brief review of the salient features of this approach. The VRC–TST approach is based on an assumed separation of modes into the "conserved" vibrational modes of the fragments and the "transitional" modes representing the overall and relative rotational modes of the fragments. The focus of the direct CASPT2 VRC–TST approach is on an accurate determination of the transitional mode contribution to the transition state partition function. This determination involves the direct evaluation, via Monte Carlo integration, of the configurational integrals arising from the classical phase space description of the partition function. The effect of any variations in the conserved modes, which is expected to be small, is neglected here.

Within the VRC–TST approach, the transition state dividing surfaces are defined in terms of a fixed distance between pivot points on each of the two reacting fragments. The variational criterion of TST then correlates with the minimization of the predicted rate constant with respect to both the location of these pivot points and the separation between them. For the present, RSR's multiple pivot points are considered,[14] corresponding to the multiple lobes of the radical orbital for such radicals. Furthermore, in each instance, both a center-of-mass pivot point and a set of radical orbital-based pivot points are considered. The center-of-mass pivot point is relevant for the large separations of importance at low temperature, while the orbital-based pivot points provide optimal dividing surfaces for the smaller separations of importance at higher temperatures. For the H atom, the pivot point is simply taken to be the H atom.

Separation distances ranging from about 8 to 15 au are considered for the center-of-mass RSR pivot point. For the orbital-based pivot points, separations correlating with minimal CH bonding separations ranging from 4.5 to 8 au are considered. Pivot point displacements from the radical atom ranging from about 0 to 2.5 au are considered. The orientation of the radical orbital pivot point displacements are optimized in preliminary calculations based on physical considerations related to the shape of the orbitals, as seen from the illustrative potential energy surfaces provided below. This range of dividing surfaces provides converged results for temperatures ranging from about 200 to 2000 K.

Infinite boundary potentials are again assumed to separate the different addition channels, and all abstraction channels are neglected. The Monte Carlo integrations over the relative orientations are generally converged to about 5%, and the present analyses are all performed at the energy and angular momentum resolved level. A uniform dynamical correction factor of 0.9 is again applied to all the VRC–TST predictions.

3. Results and Discussion

3.1. Test of Corrected CASPT2/cc-pvdz Calculations for H + HCCCH. The focus of this section will be a comparison of the potential surfaces calculated with aug-cc-pvtz and cc-

3792 *J. Phys. Chem. A, Vol. 111, No. 19, 2007*

Harding et al.
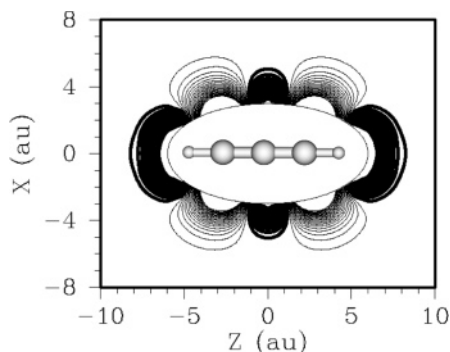
Figure 4. Two-dimensional contour plot of the three-dimensional CASPT2/aug-cc-pvtz potential surface for the H + C$_3$H$_2$ → C$_3$H$_3$ association reaction. The C$_3$H$_2$ fragment is constrained to be collinear, and the plotting plane contains this molecular axis. The heavier contours denote positive energies, and the lighter contours denote negative energies. Zero energy is defined to be the energy of the H + C$_3$H$_2$ asymptote. The contour increment is 1 kcal/mol. The blanked circle in the center hides parts of the surface that are not relevant to the association kinetics and were therefore not calculated.

pvdz basis sets with that obtained from eq 10 and of VRC−TST calculations using these three potential surfaces. Propargylene, HCCCH, was chosen for this test as it is the smallest system that exhibits significant resonance stabilization. The equilibrium geometry of propargylene is of C_2 symmetry with a CCC angle of ~175°, HCC angles of ~160°, and CCCH dihedral angles of ~140°. The B3LYP barrier to linearity is <0.5 kcal/mol. Because the purpose of this test is a comparison of the corrected, CASPT2/cc-pvdz approach with direct CASPT2 calculations using the larger aug-cc-pvtz basis, we have chosen to constrain the HCCCH fragment to be collinear to make the aug-cc-pvtz calculations more tractable. Sample calculations for the C$_2$H$_3$ + H reaction, with the C$_2$H$_3$ geometry constrained to C_{2v} geometry, suggest that such constraints have a minimal effect on the predictions for the total rate constant.

In Figure 4, we show a two-dimensional contour plot of the CASPT2/aug-cc-pvtz potential surface for H + HCCCH. This can be compared to the contour plots in Figure 5a and b, in which we show the corresponding CASPT2/cc-pvdz potential and the difference between the aug-cc-pvtz and cc-pvdz potentials. These plots demonstrate that, although the cc-pvdz potential is not as attractive as the aug-cc-pvtz potential, in all other respects the shapes of the two potentials are quite similar. The corrected, CASPT2/cc-pvdz potential, as defined by eq 10, is shown in Figure 6a and the difference between this potential and the aug-cc-pvtz potential is shown in Figure 6b. The lack of any contours in the difference plot demonstrates that the corrected, CASPT2/cc-pvdz potential and the CASPT2/aug-cc-pvtz potential agree to within better than 1 kcal/mol in the region shown.

The dynamically corrected VRC−TST predictions for the high-pressure limit rate coefficients are shown in Figure 7 for all three potential surfaces. The results for the corrected CASPT2/dz potential are within 3% of the CASPT2/atz results, further verifying the reliability of the correction procedure. Meanwhile, the uncorrected CASPT2/dz results are 20−40% below the CASPT2/atz results.

The VRC−TST formulations of refs 13 and 14 require that the pivot points lie along the linear axis. However, the radical orbitals of ^{3}CHCCH are essentially perpendicular to the linear axis, which suggests that the pivot points should be displaced from that axis. Any placement of a limited number of pivot points off the linear axis would introduce an artificial asymmetry

into the calculation. The proper generalization should involve a circular annulus of pivot points about the linear axis. The linear restriction in the pivot point location might be expected to yield an increased error in the VRC−TST predictions. To quantify this error, the rate coefficients were also obtained from trajectory simulations. These simulations found that the dynamical correction factor ranges from 0.85 to 0.88, which is indeed slightly smaller than the typical value of 0.90.[11] Subsequently, in an attempt to reduce this error, a procedure for implementing a circular annulus of pivot points was derived and applied to the ^{3}CHCCH + H reaction. This approach yielded VRC−TST rate coefficients with a corresponding dynamical correction factor of 0.90−0.94, which is more or less typical of the results for other H atom additions. A circular annulus of pivot points should be appropriate for other π radical linear species such as the OH radical.
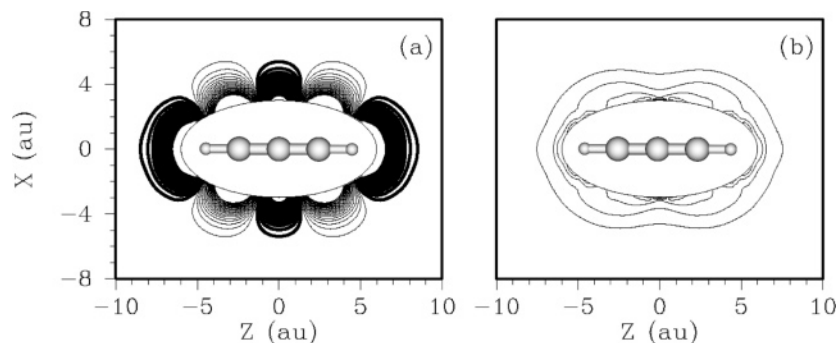
3.2. H + Allyl Radical. Preliminary calculations for the H + allyl system using a two-electron, two-orbital (2e,2o) active space revealed a problem; at large separations, the CASSCF calculation would often converge to one of two localized descriptions consisting of one double bond and one single bond. This leads to discontinuities in the potential, as the wavefunction will sometimes localize the double bond on the left and sometimes on the right. It was found that increasing the active space to include all of the valence π orbitals, i.e., (4e,4o), eliminates this problem.

A two-dimensional slice of the (4e,4o)-CASPT2/aug-cc-pvtz potential surface is shown in Figure 8. In this plot, the right side of the radical appears to be more attractive than the left. However, this perspective is simply an artifact of the plotting plane, which includes the central and right carbons but not the left carbon. In parts a and b of Figure 9, we show the corresponding CASPT2/cc-pvdz potential and the difference between the aug-cc-pvtz and cc-pvdz potentials. These plots again demonstrate that, although the cc-pvdz potential is not as attractive as the aug-cc-pvtz potential, in all other respects the shapes of the two potentials are quite similar. The corrected, CASPT2/cc-pvdz potential, as defined by eq 10, is shown in Figure 10a, and the difference between this potential and the aug-cc-pvtz potential is shown in Figure 10b. Again, the corrected CASPT2/cc-pvdz potential appears to be essentially identical to the CASPT2/aug-cc-pvtz potential.

The quantitative nature of the Δ_{adz-dz} correction was tested with direct CASPT2/aug-cc-pvdz calculations of the high-pressure combination rate constant. The resulting predictions were within 4% of those generated by applying just the orientation independent Δ_{adz-dz} correction to the CASPT2/cc-pvdz potential. In contrast, the uncorrected CASPT2/dz results are 30−50% lower.

The predicted rate coefficients for the fully corrected CASPT2/cc-pvdz potential, as defined by eq 10, are plotted in Figure 11, together with the experimental results for the H + allyl recombination. The dynamically corrected VRC−TST theoretical predictions are seen to agree with the experimental measurements of Hanning-Lee and Pilling[33] to within their error bars.

3.3. H + Propargyl Radical. Preliminary calculations using a (4e,4o) active space analogous to the H + C$_3$H$_5$ calculations described in the previous section revealed a new problem; for some orientations, the active orbitals would include the two, in-plane π orbitals in place of two of the three out-of-plane π orbitals. The most straightforward solution to this problem is to simply include in the active space all of the in-plane and out-of-plane π and π^* orbitals. In this case, that leads to a (6e,6o) active space.

Reactions of H Atoms with Hydrocarbon Radicals

J. Phys. Chem. A, Vol. 111, No. 19, 2007 **3793**

Figure 5. Potential and difference potential surfaces for H + C_3H_2 → C_3H_3. (a) CASPT2/cc-pvdz potential surface. (b) The difference potential, CASPT2/aug-cc-pvtz minus CASPT2/cc-pvdz. Plotting conventions are as in Figure 4.
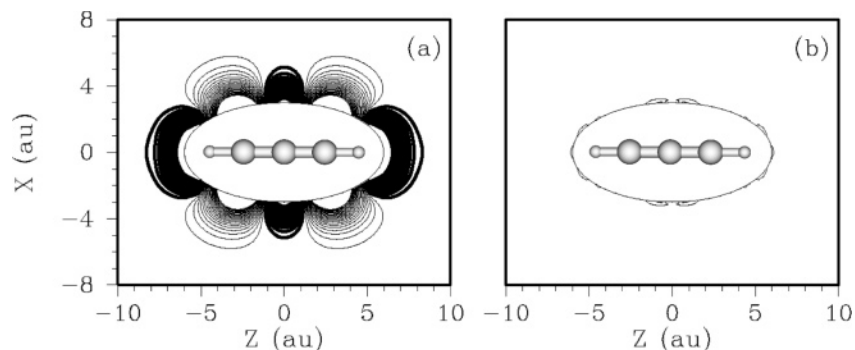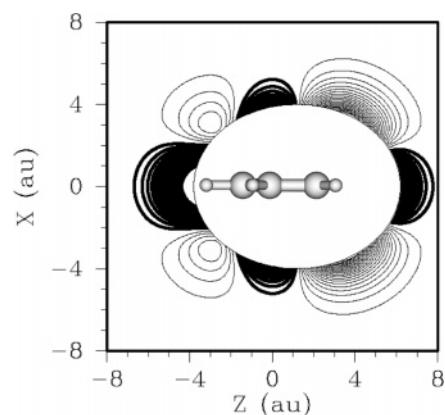

Figure 6. Corrected CASPT2/cc-pvdz potential and difference potential surfaces for H + C_3H_2 → C_3H_3. Plotting conventions are as in Figure 5.
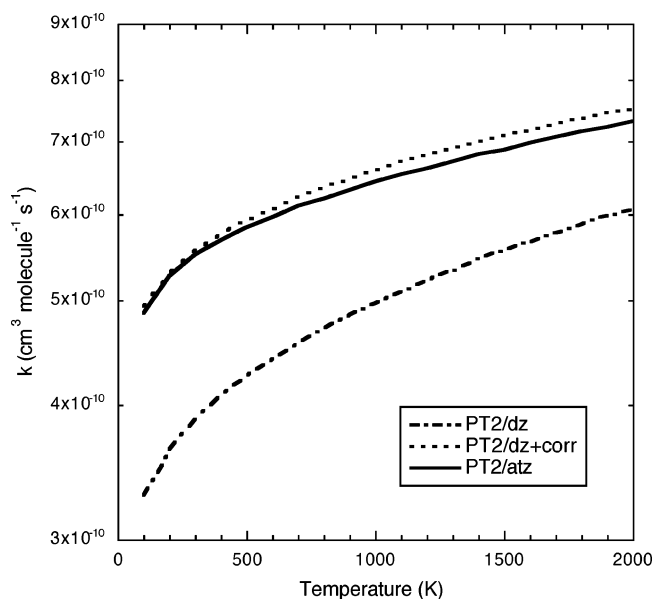
Figure 7. Plot of the high-pressure limit recombination rate constant for H + ^{3}CHCCH on three potential surfaces.

Figure 8. Two-dimensional contour plot of the three-dimensional CASPT2/aug-cc-pvtz potential surface for the H + C_3H_5 → C_3H_6 association reaction. The plotting plane is perpendicular to the plane of the molecule and includes one CC bond. Other plotting conventions are as in Figure 4.

A two-dimensional slice of the (6e,6o)-CASPT2/aug-cc-pvtz potential surface is shown in Figure 12. In parts a and b of Figure 13, we show the corresponding CASPT2/cc-pvdz potential and the difference between the aug-cc-pvtz and cc-pvdz potentials. These plots again demonstrate that, although the cc-pvdz potential is not as attractive as the aug-cc-pvtz potential, in all other respects the shapes of the two potentials are quite similar. The corrected CASPT2/cc-pvdz potential, as defined by eq 10, is shown in Figure 14a, and the difference between this potential and the aug-cc-pvtz potential is shown in Figure 14b. The apparently identical nature of the corrected CASPT2/cc-pvdz and CASPT2/aug-cc-pvtz potentials is again reinforced with rate coefficient calculations that test the Δ_{adz-dz} component of the correction.

The dynamically corrected CASPT2/cc-pvdz predictions for the recombinations to form either propyne or allene are plotted in Figure 15, together with the experimental results of Atkinson and Hudgens for the total rate.[34] Again, theory and experiment agree to within the error bars. The dominant resonance form in propargyl radical has the radical on the CH_2 (head) side. For this reason, the attractions and resulting rate coefficient are greater for the addition to form propyne. The ratio of the two rate constants is between 1.3 and 1.4 for temperatures in the 200−2500 K range.
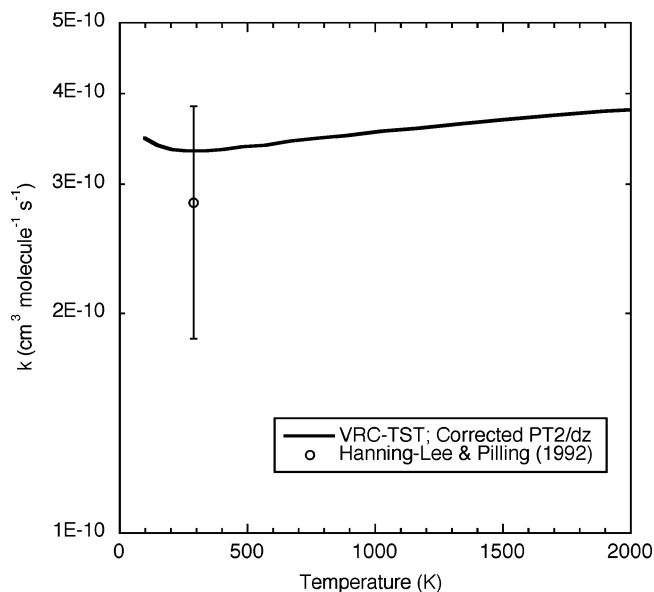
3.4. H + Methyl Propargyl Radicals. Potential surfaces for H atom combining with propargyl (CH_2CCH) and the two methyl-substituted propargyls (CH_2CCCH_3 and CH_3CHCCH) are compared in parts a, b, and c, respectively, of Figure 16. The plots illustrate the steric interactions between the methyl substituent on the propargyl radical and the incoming hydrogen atom. These plots suggest that the methyl group will have a
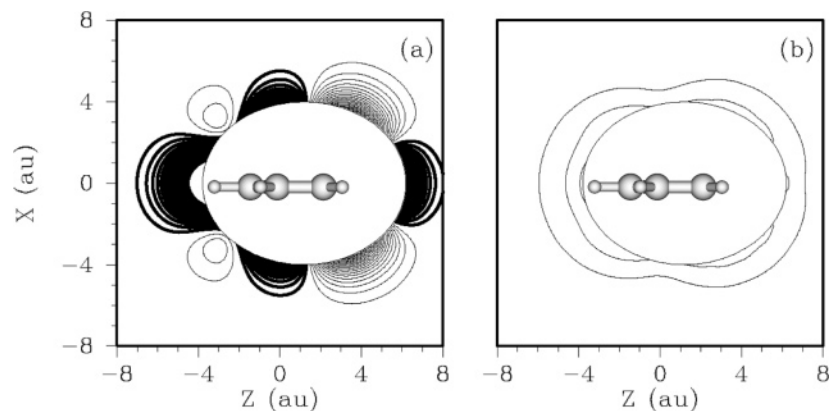
Figure 9. Potential and difference potential surfaces for H + $C_3H_5 \rightarrow C_3H_6$. (a) CASPT2/cc-pvdz potential surface. (b) The difference potential, CASPT2/aug-cc-pvtz minus CASPT2/cc-pvdz. Plotting conventions are as in Figure 7.
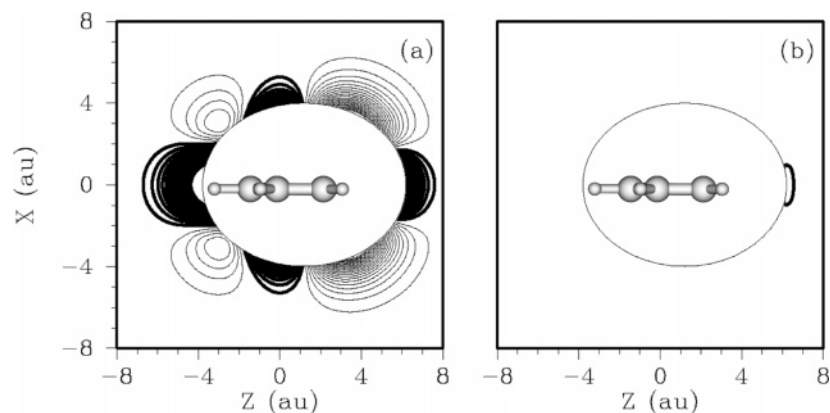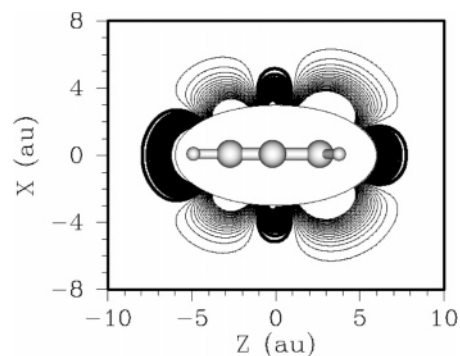

Figure 10. Corrected CASPT2/cc-pvdz potential and difference potential surfaces for H + $C_3H_5 \rightarrow C_3H_6$. Plotting conventions are as in Figure 8.

Figure 11. Plot of the high-pressure limit recombination rate constant for H + CH_2CHCH_2.

Figure 12. Two-dimensional contour plot of the three-dimensional CASPT2/aug-cc-pvtz potential surface for the H + $C_3H_3 \rightarrow C_3H_4$ association reaction. The plotting plane is perpendicular to the plane of the molecule and includes the three carbons. Other plotting conventions are as in Figure 4.

significant (hindering) effect on the adjacent radical site but little effect on the radical site at the opposite end of the molecule.

These qualitative conclusions are confirmed by the TST calculations, the results of which are shown in Figure 17. The rate coefficients to add to the unsubstituted sides of the methyl-substituted propargyls are essentially identical to that for the corresponding addition in propargyl. In contrast, the rate coefficient for adding to the methyl-substituted side of CH_3-CHCCH is about a factor of 2 lower than the corresponding

propargyl case, while that for adding to the methyl-substituted side of CH_2CCCH_3 is about a factor of 3 lower. The greater steric effect for the latter case arises because the attractive potential is weaker for addition to the tail side of the radical. As a result, the transition state tends to be at shorter separations for the tail side, and steric interactions have a greater effect on the rate coefficient. The greater steric effect for the CH_2CCCH_3 + H $\rightarrow$ CH_2CCHCH_3 case is for the smaller component of the addition rate. Thus, the total rate coefficient for the two methyl-substituted propargyls are nearly identical, with both being about 1.4 times smaller than the H + propargyl rate coefficient.

3.5. H + CH_2CCCH and CH_2CCCCH. Contour plots of the potential surfaces for reaction of H atom with CH_2CCCCH and CH_2CCCH are shown in parts a and b, respectively, of Figure 18. Note that, for CH_2CCCH, the radical orbital is in

Reactions of H Atoms with Hydrocarbon Radicals

J. Phys. Chem. A, Vol. 111, No. 19, 2007 **3795**
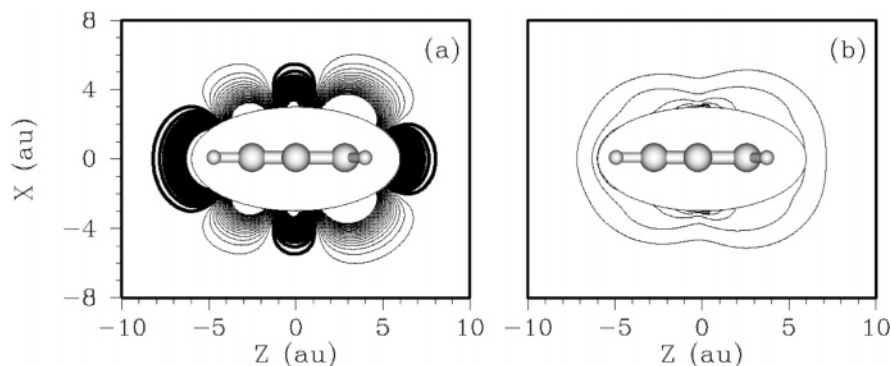
Figure 13. Potential and difference potential surfaces for H + C$_3$H$_3$ → C$_3$H$_4$. (a) CASPT2/cc-pvdz potential surface. (b) The difference potential, CASPT2/aug-cc-pvtz minus CASPT2/cc-pvdz. Plotting conventions are as in Figure 12.
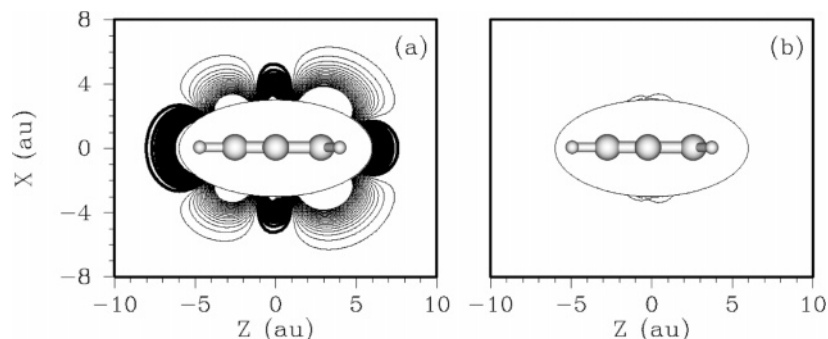

Figure 14. Corrected CASPT2/cc-pvdz potential and difference potential surfaces for H + C$_3$H$_3$ → C$_3$H$_4$. Plotting conventions are as in Figure 12.
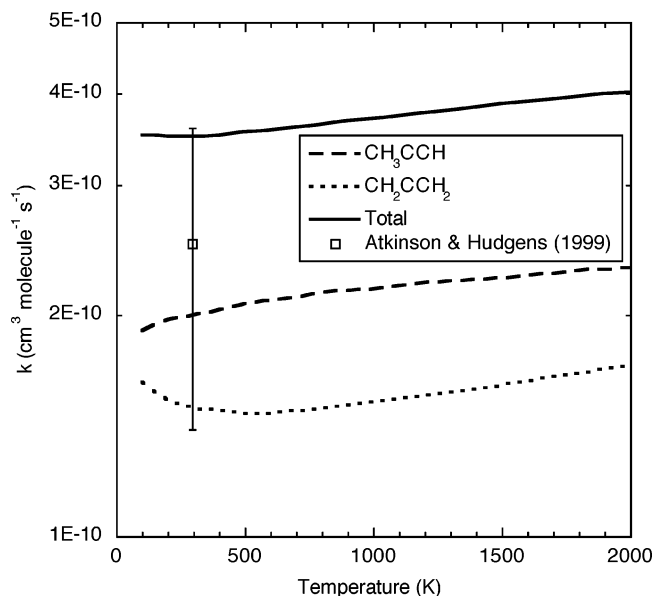
Figure 15. Plot of the high-pressure limit recombination rate constant for H + CH$_2$CCH to make propyne (CH$_3$CCH) and allene (CH$_2$CCH$_2$).

the plane of the molecule, while for CH$_2$CCCCH, it is in a π orbital perpendicular to the plane of the molecule. This difference has important effects on the two reactions. The perpendicular, radical π orbital of CH$_2$CCCCH is more accessible to the approaching H atom, while the CH bonds of the CH$_2$ moiety noticeably hinder approach to the in-plane, radical π orbital of CH$_2$CCCH. However, the in-plane π orbital of CH$_2$-CCCH allows for the possibility of a direct, barrierless abstraction reaction forming H$_2$ and diacetylene. Evidence for this pathway can be seen in the attractive contours on the right side of Figure 18b. Treatment of this abstraction reaction is outside the scope of this work.
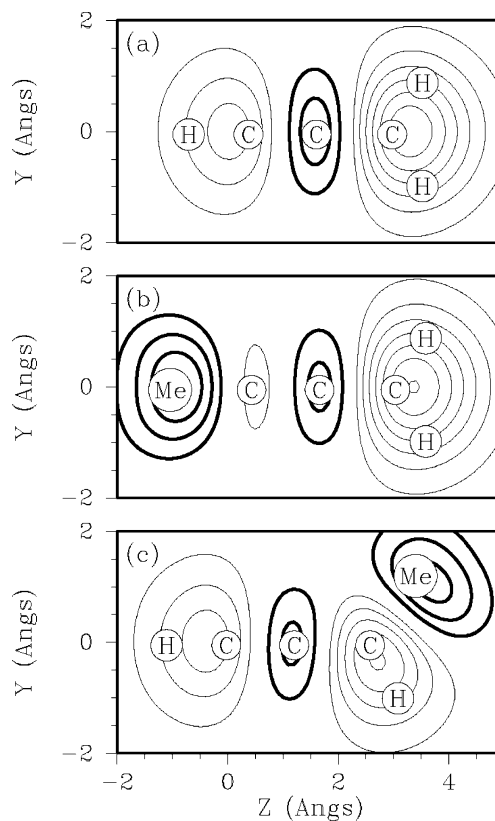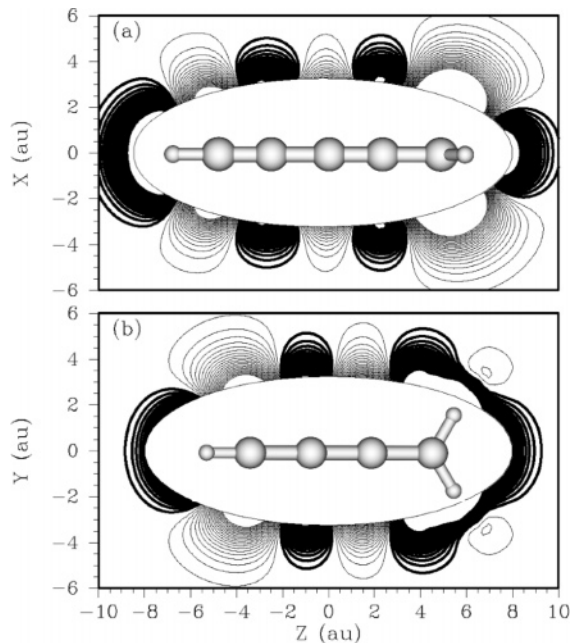

Figure 16. Contour plots of the potential surfaces for the reactions: (a) H + CH$_2$CCH → C$_3$H$_4$, (b) H + CH$_2$CCCH$_3$ → C$_4$H$_6$, (c) H + CH$_3$CHCCH → C$_4$H$_6$. The plotting planes are parallel to the symmetry planes of the molecules but displaced by 2.5 Å. Other plotting conventions are as in Figure 4.

The predicted high-pressure recombination rate constants for H adding to CH$_2$CCH, CH$_2$CCCH, and CH$_2$CCCCH are plotted in Figure 19. The total addition rates for the odd C members in
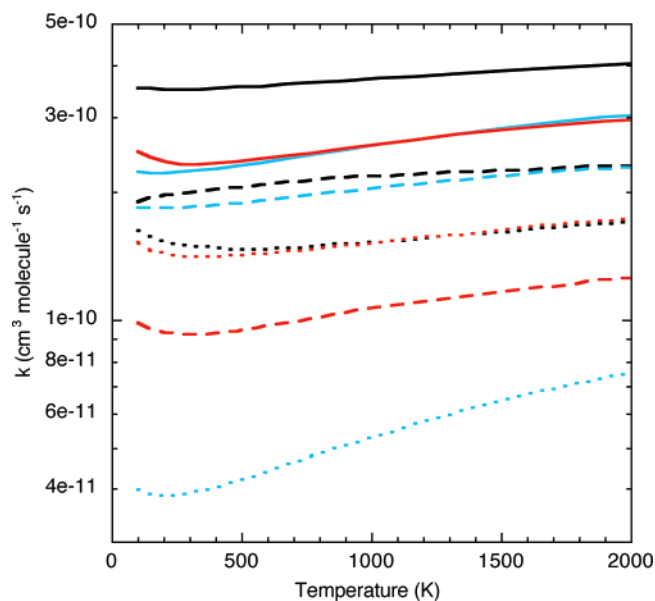
Figure 17. Plot of the high-pressure limit recombination rate constants for H + CH$_2$CCH (black), H + CH$_2$CCCH$_3$ (blue), and H + CH$_3$-CHCCH (red). The solid lines denote the total rates, the dashed lines denote the rates to add to the head of the radical (to form CH$_3$CCH, CH$_3$CCCH$_3$, and CH$_3$CH$_2$CCH), and the dotted lines denote the rates to add to the tail of the radical (to form CH$_2$CCH$_2$, CH$_2$CCHCH$_3$, and CH$_3$CHCCH$_2$).

Figure 18. Contour plots of the potential surfaces for the reactions: (a) H + CH$_2$CCCCH → C$_5$H$_4$ and (b) H + CH$_2$CCCH → C$_4$H$_4$. The plotting plane for (a) is perpendicular to the plane of the molecule. For (b), the plotting plane is in the plane of the molecule. Other plotting conventions are as in Figure 4.

the series (CH$_2$CCH and CH$_2$CCCCH) are essentially identical, suggesting that the presence of one more addition site in the CH$_2$CCCCH case is balanced by a decrease in the attractiveness due to the greater resonance stabilization and/or by the presence of additional steric repulsions for each of the channels. In contrast, the total addition rate for CH$_2$CCCH is about a factor of 1.7 lower. This decrease for the even C species, CH$_2$CCCH, is largely due to the increased steric repulsion for addition in the plane as opposed to out of the plane. In particular, the addition to the "central" C in CH$_2$CCCH to form CH$_2$CHCCH
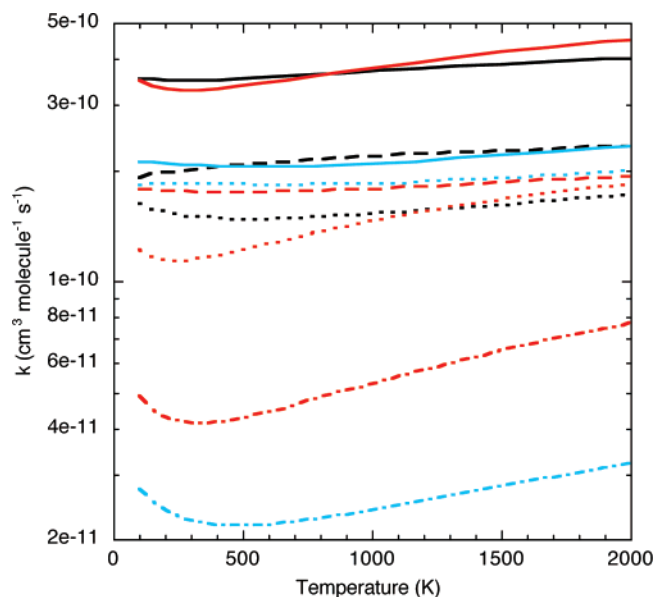
Figure 19. Plot of the high-pressure limit recombination rate constants for H + CH$_2$CCH (black), H + CH$_2$CCCH (blue), and H + CH$_2$CCCCH (red). The solid lines denote the total rates, the dashed lines denote the rates to add to the head of the radical (to form CH$_3$-CCH and CH$_3$CCCCH), the dotted lines denote the rates to add to the tail of the radical (to form CH$_2$CCH$_2$, CH$_2$CCCH$_2$, and CH$_2$CCCCH$_2$), and the dot−dashed lines denote the rates to add to a central C (to form CH$_2$CHCCH and CH$_2$CCHCCH).
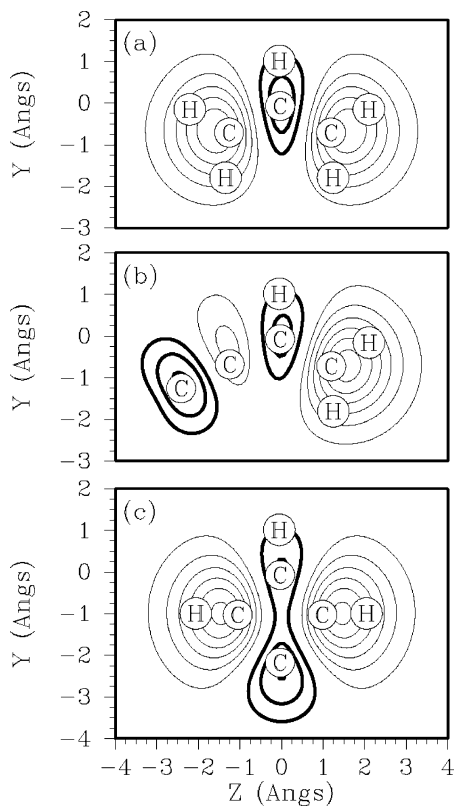
is a factor of 6−8 less than the addition to either end of CH$_2$-CCH and is even a factor of 2−3 less than the central addition in CH$_2$CCCCH.

For the C3 and C5 cases of the CH$_2$C$_n$CH series (CH$_2$CCH and CH$_2$CCCCH), the dominant resonance structure has the radical on the CH$_2$ terminal C, as seen by the increased attractiveness for the addition to the CH$_2$ site in Figures 12 and 18a. For this reason, the rates to add to the CH$_2$ site for these two cases are significantly greater than those for the other sites. The rate to add to the central C in the C5 case is especially small because it has the least attractive potential and it has the most steric hindrance.

For the C4 case (CH$_2$CCCH), the dominant resonance structure is somewhat less clear. With B3LYP/6-31G* calculations, the structure has C_{2v} symmetry, implying that the dominant resonance structure has the radical on the C adjacent to the CH$_2$ C. This C_{2v} structure is employed in the present rate calculations. In contrast, the CCSD(T)/TZ calculations of Allen and co-workers[35] suggest that the molecule has C_s symmetry with the terminal C in the CH group being the dominant radical site. Our own CASPT2 calculations suggest that the optimal structure is in fact strongly dependent on basis set, with the C_s to C_{2v} excitation energy varying from 1.1 to 0.04 kcal/mol as the basis is varied from aug-cc-pvdz to aug-cc-pvqz. The reality is that the potential for the C_{2v} to C_s distortions is very flat. The contour plot of Figure 18b suggests that the present corrected CASPT2/dz approach places the radical predominantly on the terminal CH group. Thus, the predicted rate coefficient for the H addition to the terminal CH group in the C4 case is slightly greater than those for the corresponding additions in the C3 and C5 case, where the dominant radical site was on the CH$_2$ terminus.

It is perhaps worth noting that our predictions for the total rate are expected to be only weakly dependent on the assumed molecular structure. For example, we have performed calculations for the addition to add an H atom to C$_2$H$_3$ assuming a C_{2v} structure for C$_2$H$_3$. These calculations yield an essentially

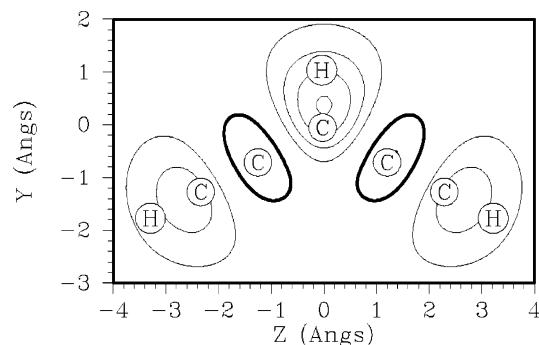Reactions of H Atoms with Hydrocarbon Radicals

J. Phys. Chem. A, Vol. 111, No. 19, 2007 **3797**

Figure 20. Contour plots of the potential surfaces for the reactions: (a) H + CH$_2$CHCH$_2$ → C$_3$H$_6$, (b) H + *i*-C$_4$H$_5$ → C$_4$H$_6$, (c) H + *cyclo*-C$_4$H$_5$ → C$_4$H$_6$. The plotting planes are parallel to the carbon atom planes but displaced by 2.5 Å. Only the atoms in the same plane as the carbons are shown. Other plotting conventions are as in Figure 4.
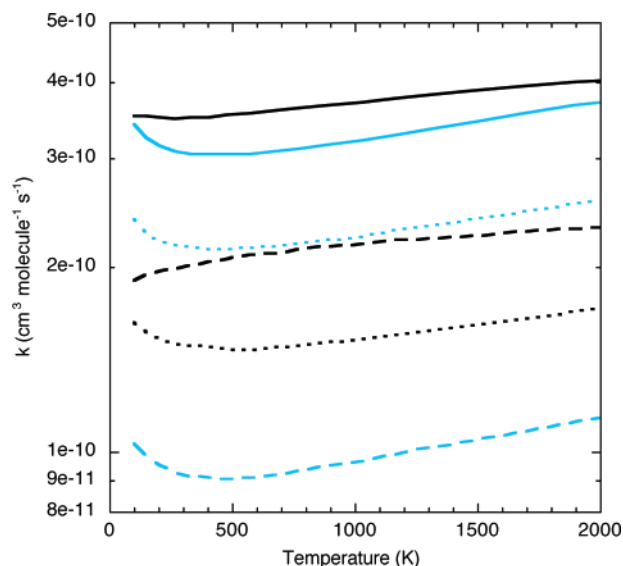

Figure 22. Contour plots of the potential surfaces for the reaction, H + CHCCHCCH → C$_5$H$_4$. The plotting plane is parallel to the molecular plane but displaced by 2.5 Å. Other plotting conventions are as in Figure 4.
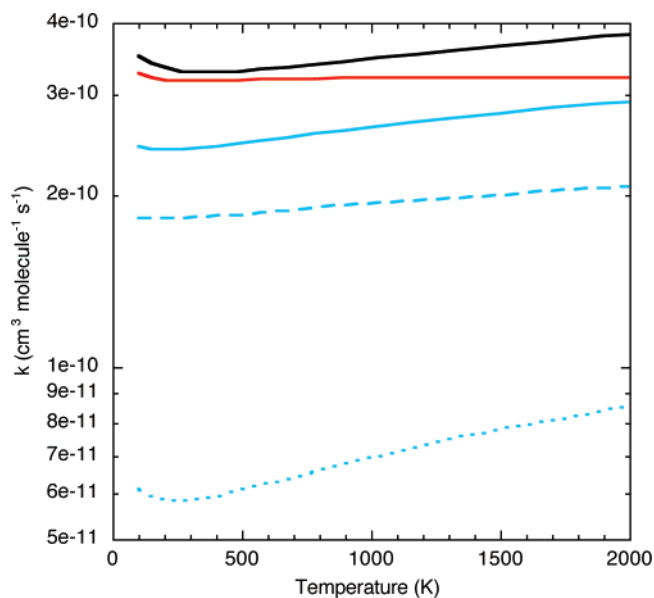
Figure 21. Plot of the high-pressure limit recombination rate constants for H + allyl (black), H + *i*-C$_4$H$_5$ (blue), and H + *cyclo*-C$_4$H$_5$ (red). The solid lines denote the total rates, the blue dashed and dotted lines denote the rates to form CH$_3$CHCCH$_2$ and CH$_2$CHCHCH$_2$, respectively.

Figure 23. Plot of the high-pressure limit recombination rate constants for H + CH$_2$CCH (black) and H + CHCCHCCH (blue). The solid lines denote the total rates, the dashed lines denote the rates to add to the "CH$_2$" portion of the radical (to form CH$_3$CCH or CHCCH$_2$CCH), and the dotted lines denote the rates to add to the CH sites (to form CH$_2$CCH$_2$ or CH$_2$CCHCCH).

identical total rate coefficient to ones performed for the proper C_s structure. In contrast, however, the predicted branching between different addition sites can depend on the assumed structure. For example, for the C_{2v} C$_2$H$_3$ structure the "front" and "back" addition rates are identical, whereas for the proper

C_s case, they differ substantially. Thus, the uncertainty in the proper structure for C$_4$H$_3$ implies that our predicted branching between formation of CH$_2$CHCCH and CH$_2$CCCH$_2$ may not be particularly accurate.

3.6. H + *i*-C$_4$H$_5$ and H + *cyclo*-C$_4$H$_5$. Contour plots of the potential surfaces for H + *i*-C$_4$H$_5$ and H + *cyclo*-C$_4$H$_5$ are shown in parts b and c, respectively, of Figure 20. Also shown for comparison is a plot of H + allyl using the same plotting conventions because these two radicals can be considered as substituted allyl radicals. The biggest difference between the three plots is in the left side of the H + *i*-C$_4$H$_5$ potential, where it is clear that the out-of-plane CH bonds (not shown in the plot) are hindering the attack on the left radical site. The other radical sites all show a similar degree of attraction, but with the H + *cyclo*-C$_4$H$_5$ and right side of the H + *i*-C$_4$H$_5$ being slightly more attractive than the H + allyl site. Similarly, the CH bond strength in cyclobutene (90.0 kcal/mol) is greater than that in 1,3-butadiene (88.8 kcal/mol), which is greater than that in propene (86.7 kcal/mol). The suggestion from these plots then is that the H + *i*-C$_4$H$_5$ combination to form 1,3-butadiene should be significantly slower than the addition to form methyl-
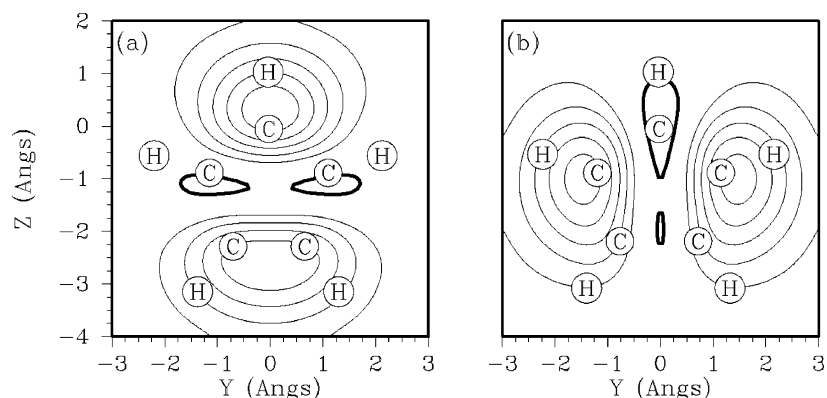
Figure 24. Contour plots of the potential surfaces for the reaction H + *cyclo*-C$_5$H$_5$ → C$_5$H$_6$: (a) ^{2}B$_1$ state and (b) ^{2}A$_2$ state. The plotting planes are parallel to the molecular plane but displaced by 2.5 Å. Other plotting conventions are as in Figure 4.
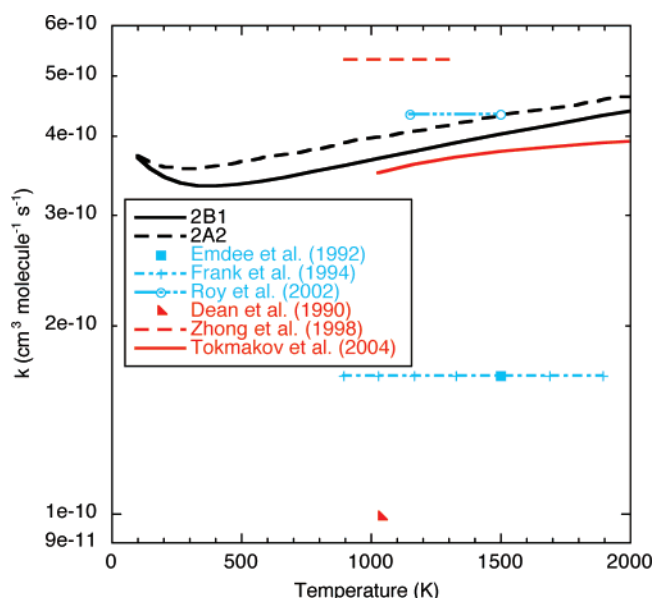

**Figure 25.** Plot of the high-pressure limit recombination rate constant for H + cyclopentadienyl. Black denotes the present theoretical predictions for the 2B$_1$ (solid) and 2A$_2$ (dashed) states of cyclopentadienyl. The blue symbols and lines denote the experimental results from refs 37, 38, and 39. The red symbols denote prior theoretical results from refs 40, 41, and 42.

allene. The H + allyl and H + *cyclo*-C$_4$H$_5$ rates should be similar, both being about twice the H + *i*-C$_4$H$_5$ → methyl-allene rate.

The plots in Figure 21 of the predicted high-pressure recombination rate constants for H adding to allyl, *i*-C$_4$H$_5$, and *cyclo*-C$_4$H$_5$, verify these expectations. Also, the H + *i*-C$_4$H$_5$ → methyl-allene combination rate is seen to be slightly greater than half the H + allyl rate, which is due to the increased attractiveness of the potential. However, the H + *cyclo*-C$_4$H$_5$ combination rate is slightly less than the H + allyl combination rate, even though its minimum energy path potential is slightly more attractive. This result is due to the greater steric hindrance in the H + *cyclo*-C$_4$H$_5$ case, which becomes increasingly important as the temperature increases and the transition state separations decrease.

3.7. H + CHCCHCCH. A contour plot of the potential surface for H + CHCCHCCH combination is shown in Figure 22. Three reactive sites are found. Addition to the central carbon leads to 1,4-pentadiyne, while addition to either end leads to a substituted allene. Comparison with Figure 16a indicates that, for both of the distinct addition sites, the H + CHCCHCCH
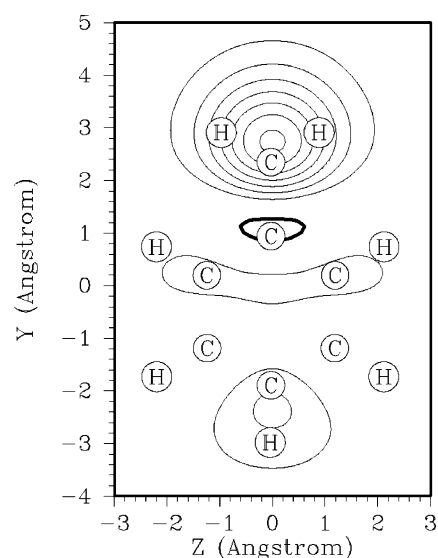

Figure 26. Contour plots of the potential surfaces for the reaction, H + benzyl → C$_7$H$_8$, The plotting plane is parallel to the molecular plane but displaced by 2.5 Å. Other plotting conventions are as in Figure 4.

potential is less attractive than the corresponding site in the H + CH$_2$CCH potential. This decrease in attractiveness is, at least in part, related to the greater resonance stabilization in the CHCCHCCH case. Also, the steric hindrance for addition to the central C in CHCCHCCH is much greater than for the addition to the CH$_2$ site in CH$_2$CCH.

The high-pressure limit rate coefficients for the H + CHCCHCCH combination are plotted in Figure 23, together with the related rate coefficients for the H + CH$_2$CCH reaction. As expected, the rate coefficient for addition to the central site in CHCCHCCH is much lower than (∼a factor of 2) the rate coefficient for adding to the CH$_2$ site in propargyl. However, the total rate coefficient to add to the CH sites in CHCCHCCH is ∼50% higher than that for adding to the CH site in CH$_2$-CCH. This increase for the CHCCHCCH case is due to the presence of two separate CH sites in that case. Overall, the total rate coefficient for H + CHCCHCCH is still significantly lower than that for H + CH$_2$CCH.

3.8. H + Cyclopentadienyl Radical. For a D_{5h} constrained geometry, cyclopentadienyl radical will have a degenerate, ^{2}E″$_1$, ground electronic state. As has been discussed in the literature,[36] the Jahn−Teller effect causes the molecule to distort from D_{5h} to C_{2v}, and the two degenerate electronic states split into

Reactions of H Atoms with Hydrocarbon Radicals

J. Phys. Chem. A, Vol. 111, No. 19, 2007 **3799**
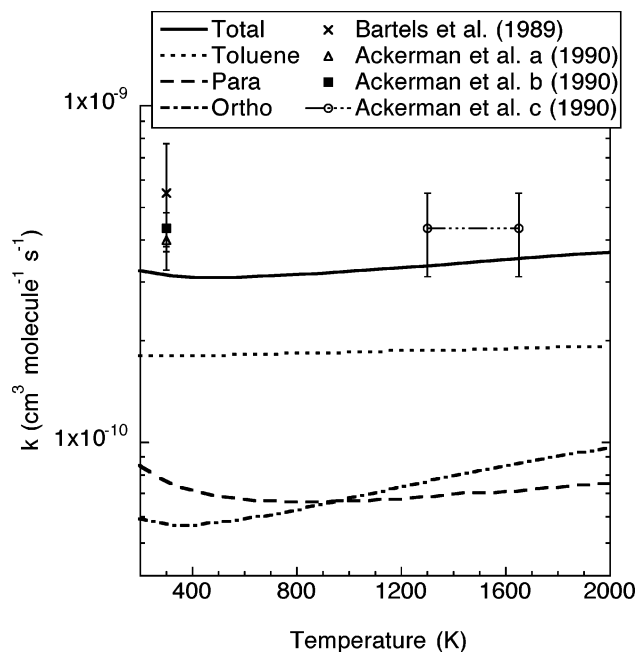
Figure 27. Plot of the high-pressure limit recombination rate constant for H + benzyl radical. The lines denote the present theoretical predictions, while the symbols denote the experimental results from refs 43, 44.
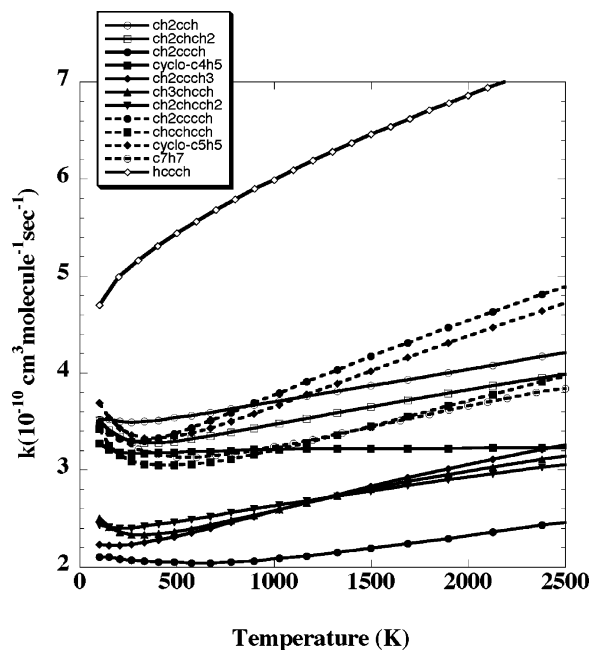

Figure 28. Plot of the total, high-pressure limit, recombination rate constants for H with RSR's 1−12.

slightly nondegenerate $^2B_1$ and $^2A_2$ states, commonly depicted as follows:
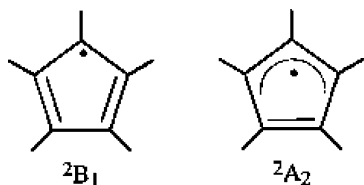
Contour plots of potential surfaces for H addition to each of these two states are shown in Figure 24. These plots make clear that the above structures do not well represent the electronic structure of these two states. Both clearly have significant radical character on the lower two carbon atoms, something that is missing from the depictions shown above. The contour plots suggest that the overall reactivity of the two states should be quite similar.

The presence of these two nearly degenerate electronic states presents some complications for the rate calculations. For example, when considering the apparently repulsive portions of the potential for the $^2B_1$ state, we instead find that the direct sampling says it is attractive. In essence, the direct sampling is finding the adiabatically lowest potential, which happens to correlate with the $^2A_2$ electronic state. In the rate calculations, we make an electronically adiabatic assumption and simply take the lowest potential energy for each geometry sampled. Nevertheless, this still introduces some difficulties in the determination of the optimal dividing surfaces, with an expected increase in the uncertainties of the predictions of about 10−20%.

As an alternative to calculating separate $^2B_1$ and $^2A_2$ rate coefficients, we have also performed the calculations assuming D_{5h} symmetry. For the latter geometry, the interaction with the H atoms yields a purely attractive singlet state and a separate purely repulsive singlet state. The rates calculated for the $^2B_1$ and $^2A_2$ states agree with that calculated for the D_{5h} case (to within ∼10%) when we assume that the two separate singlet

electronic states retain a statistical distribution. If instead they are assumed to be unmixed, the repulsive state makes no contribution, and then the D_{5h} rate is about 1.5 times lower. This deviation suggests that our predictions for this reaction may be sensitive to the extent of the electronic mixing of the two lowest singlet states at shorter separation.

The predictions for the H + cyclopentadienyl combination rate in the $^2B_1$ and $^2A_2$ states are illustrated in Figure 25, together with the available experimental data[37−39] and prior theoretical predictions.[40−42] The present predictions are in good agreement with the most recent, and only direct, experimental study of this reaction.[39] The prior theoretical estimates of Dean et al.[40] and Bozzelli and co-workers[41] appear to be purely empirical, and so it is perhaps not too surprising that they are both significantly in error. The theoretical predictions of Lin and co-workers[42] are based on scaled B3LYP calculations and consider only harmonic vibrators even for the transitional modes. Our experience suggests that each of these assumptions can lead to errors of a factor of 2 or more. Thus, the close agreement between their predictions and the present ones would appear to be somewhat fortuitous.

3.9. H + Benzyl Radical. A contour plot for the potential surface for H + benzyl is shown in Figure 26. Four distinct reactive sites are visible, one each leading to toluene and *p*-isotoluene and two equivalent sites leading to *o*-isotoluene. The site leading to toluene is clearly the most attractive.

The predicted rate H + benzyl combination rate coefficients from ref 22 are illustrated in Figure 27. Again, the total rate constant is in good agreement with the available experimental data.[43,44] The rate to add to the CH_2 site, to form toluene, is similar to the rate to add to the CH_2 side of propargyl radical. The rates to form the para and ortho channels are each about $^1/_2$ of the rate to form toluene. The large magnitude for the branching to form *ortho*-toluene is a little surprising given the much weaker attractiveness (cf. Figure 26) of its potential. Apparently, the presence of two addition sites for this channel offsets the decreased attractiveness of the potential.

4. Concluding Remarks.

The major conclusions from this study can be summarized as follows:

(1) Calculational method: Combination reactions involving resonance-stabilized radicals present new challenges. In our previous study of H atom + nonresonance-stabilized, hydrocarbon radical reactions, we found accurate results could be obtained from small basis set, small active space CASPT2 potential surfaces to which a simple, one-dimensional correction is added. Furthermore, it was found that a single, one-dimensional correction (for all nonresonance-stabilized hydrocarbon radicals) was adequate. We find this approach to be inadequate for reactions involving RSR's. Two modifications are required to get accurate rate coefficients for reactions involving RSR's. First, larger active spaces are needed such that the dominant resonance effects are included in the active space. Second, different correction potentials are needed for each radical site on each RSR. With these two straightforward modifications, it is demonstrated that accurate predictions of combination rates for reactions involving RSR's can be made.

(2) H + R Association Rate Coefficients: The calculated high-pressure limit total H + R combination rates for RSR's **1−12** over the temperature range of 200−2000 K are well fit (±5%) by the following expressions:

$$k(H + {}^3CHCCH \rightarrow CH_2CCH) =$$
$$4.42 \times 10^{-10} \, (T/298)^{0.220} \exp(43.7/T)$$

$$k(H + CH_2CCH \rightarrow products) =$$
$$2.98 \times 10^{-10} \, (T/298)^{0.147} \exp(46.3/T)$$

$$k(H + CH_2CCH \rightarrow CH_3CCH) =$$
$$1.90 \times 10^{-10} \, (T/298)^{0.102} \exp(15.7/T)$$

$$k(H + CH_2CCH \rightarrow CH_2CCH_2) =$$
$$1.10 \times 10^{-10} \, (T/298)^{0.206} \exp(87.1/T)$$

$$k(H + CH_2CHCH_2 \rightarrow CH_3CHCH_2) =$$
$$2.64 \times 10^{-10} \, (T/298)^{0.176} \exp(63.0/T)$$

$$k(H + CH_2CCCH \rightarrow products) =$$
$$1.55 \times 10^{-10} \, (T/298)^{0.192} \exp(81.4/T)$$

$$k(H + CH_2CCCH \rightarrow CH_2CCCH_2) =$$
$$1.52 \times 10^{-10} \, (T/298)^{0.125} \exp(52.9/T)$$

$$k(H + CH_2CCCH \rightarrow CH_2CHCCH) =$$
$$9.98 \times 10^{-12} \, (T/298)^{0.556} \exp(232.9/T)$$

$$k(H + CH_2CHCCH_2 \rightarrow products) =$$
$$2.01 \times 10^{-10} \, (T/298)^{0.184} \exp(52.4/T)$$

$$k(H + CH_2CHCCH_2 \rightarrow CH_3CHCCH_2) =$$
$$1.63 \times 10^{-10} \, (T/298)^{0.119} \exp(33.6/T)$$

$$k(H + CH_2CHCCH_2 \rightarrow CH_2CHCHCH_2) =$$
$$4.10 \times 10^{-11} \, (T/298)^{0.359} \exp(103/T)$$

$$k(H + CH_3CHCCH \rightarrow products) =$$
$$1.74 \times 10^{-10} \, (T/298)^{0.262} \exp(85.2/T)$$

$$k(H + CH_3CHCCH \rightarrow CH_3CHCCH_2) =$$
$$1.08 \times 10^{-10} \, (T/298)^{0.227} \exp(78.0/T)$$

$$k(H + CH_3CHCCH \rightarrow CH_3CH_2CCH) =$$
$$6.68 \times 10^{-11} \, (T/298)^{0.307} \exp(93.6/T)$$

$$k(H + CH_3CCCH_2 \rightarrow products) =$$
$$1.69 \times 10^{-10} \, (T/298)^{0.288} \exp(80.9/T)$$

$$k(H + CH_3CCCH_2 \rightarrow CH_3CCCH_3) =$$
$$1.51 \times 10^{-10} \, (T/298)^{0.205} \exp(57.3/T)$$

$$k(H + CH_3CCCH_2 \rightarrow products) =$$
$$2.22 \times 10^{-11} \, (T/298)^{0.596} \exp(163/T)$$

$$k(H + cyc\text{-}C_4H_5 \rightarrow cyc\text{-}C_4H_6) =$$
$$3.16 \times 10^{-10} \, (T/298)^{0.0108} \exp(1.63/T)$$

$$k(H + CH_2CCCCH \rightarrow products) =$$
$$2.30 \times 10^{-10} \, (T/298)^{0.330} \exp(104/T)$$

$$k(H + CH_2CCCCH \rightarrow CH_3CCCCH) =$$
$$1.42 \times 10^{-10} \, (T/298)^{0.145} \exp(58.1/T)$$

$$k(H + CH_2CCCCH \rightarrow CH_2CCCCH_2) =$$
$$8.14 \times 10^{-11} \, (T/298)^{0.401} \exp(98.3/T)$$

$$k(H + CH_2CCCCH \rightarrow CH_2CCHCCH) =$$
$$1.88 \times 10^{-11} \, (T/298)^{0.681} \exp(227/T)$$

$$k(H + CHCCHCCH \rightarrow products) =$$
$$2.11 \times 10^{-10} \, (T/298)^{0.268} \exp(108/T)$$

$$k(H + CHCCHCCH \rightarrow CH_2CCHCCH) =$$
$$1.52 \times 10^{-10} \, (T/298)^{0.251} \exp(101/T)$$

$$k(H + CHCCHCCH \rightarrow CHCCH_2CCH) =$$
$$5.94 \times 10^{-11} \, (T/298)^{0.309} \exp(126/T)$$

$$k(H + cyc\text{-}C_5H_5 \, (^2A_2) \rightarrow C_5H_6) =$$
$$2.60 \times 10^{-10} \, (T/298)^{0.281} \exp(90.2/T)$$

$$k(H + cyc\text{-}C_5H_5 \, (^2B_1) \rightarrow C_5H_6) =$$
$$2.19 \times 10^{-10} \, (T/298)^{0.333} \exp(122/T)$$

$$k(H + cyc\text{-}C_7H_7 \rightarrow products) =$$
$$2.24 \times 10^{-10} \, (T/298)^{0.223} \exp(95.4/T)$$

$$k(H + cyc\text{-}C_7H_7 \rightarrow toluene) =$$
$$1.65 \times 10^{-10} \, (T/298)^{0.0731} \exp(25.9/T)$$

$$k(H + cyc\text{-}C_7H_7 \rightarrow p\text{-}isotoluene) =$$
$$4.45 \times 10^{-11} \, (T/298)^{0.222} \exp(154/T)$$

$$k(H + cyc\text{-}C_7H_7 \rightarrow o\text{-}isotoluene) =$$
$$2.73 \times 10^{-11} \, (T/298)^{0.594} \exp(210/T)$$

where the rate coefficients are in cm^3 molecule^{-1} s^{-1} and the temperature is in K.

The total rates for hydrogen atom combination with RSR's **1−12**, shown in Figure 28, fall in the range $2-7 \times 10^{-10}$ cm^3 mol^{-1} s^{-1}, with propargylene being the fastest and CH$_2$CCCH the slowest. The propargylene reaction is significantly faster than any of the others probably because there are two radical electrons. All of the combination rates are predicted to have

Reactions of H Atoms with Hydrocarbon Radicals

J. Phys. Chem. A, Vol. 111, No. 19, 2007 **3801**

small positive dependences on temperature except H + *cyclo*-C$_4$H$_5$, which is predicted to be essentially independent of temperature.

We found that the rate coefficients calculated for H + propargyl and H + allyl combinations provided good building blocks for interpreting the kinetics of many of the larger RSRs. As in our previous study of H atom combinations with alkyl radicals, we find a methyl substituent, adjacent to a radical site, exerts a steric hindrance that decreases the rate for addition to that site by approximately a factor of 2 (more for less reactive sites) over the parent. As discussed in Section 3, the relatively slow rates for CH$_2$CCCH, CH$_3$CCCH$_2$, CH$_2$CHCHCCH$_2$, and CH$_3$-CHCCH can all be understood on the basis of steric interactions, hindering approach to the radical sites.

References and Notes

(1) Miller, J. A.; Melius, C. F. *Combust. Flame* **1992**, *91*, 21.

(2) Melius, C. F.; Miller, J. A.; Evleth, E. M. *Proc. Combust. Inst.* **1992**, *24*, 621.

(3) Pope, C. J.; Miller, J. A. *Proc. Combust. Inst.* **2000**, *28*, 1519.

(4) Miller, J. A.; Klippenstein, S. J. *J. Phys. Chem. A* **2001**, *105*, 7254.

(5) Miller, J. A.; Klippenstein, S. J. *J. Phys. Chem. A* **2003**, *107*, 7783.

(6) Miller, J. A.; Pilling, M. J.; Troe, J. *Proc. Combust. Inst.* **2005**, *30*, 43.

(7) Melius, C. F.; Colvin, M. E.; Marinov, N. M.; Pitz, W. J.; Senkan, S. M. *Proc. Combust. Inst.* **1998**, *26*, 685.

(8) Lindstedt, P.; Maurice, L.; Meyer, M. *Faraday Discuss.* **2001**, *119*, 409.

(9) Howard, J. B.; Richter, H. *Prog. Energy Combust. Science* **2000**, *26*, 565.

(10) Lamprecht, A.; Atakan, B.; Kohse-Hoinghaus, K. *Combust. Flame* **2000**, *122*, 483.

(11) Harding, L. B.; Georgievskii, Y.; Klippenstein, S. J. *J. Phys. Chem. A* **2005**, *109*, 4646.

(12) Klippenstein, S. J.; Georgievskii, Y.; Harding, L. B. *Phys. Chem. Chem. Phys.* **2006**, *8*, 1133.

(13) Klippenstein, S. J. *J. Chem. Phys.* **1992**, *96*, 367.

(14) Georgievskii, Y.; Klippenstein, S. J. *J. Phys. Chem. A* **2003**, *107*, 9776.

(15) Werner, H.-J. *Mol. Phys.* **1996**, *89*, 645.

(16) Celani, P.; Werner, H.-J. *J. Chem. Phys.* **2000**, *112*, 5546.

(17) Taatjes, C. A.; Klippenstein, S. J.; Hansen, N.; Miller, J. A.; Cool, T. A.; Wang, J.; Law, M. E.; Westmoreland, P. R. *Phys. Chem. Chem. Phys.* **2005**, *7*, 806.

(18) Hansen, N.; Klippenstein, S. J.; Taatjes, C. A.; Miller, J. A.; Wang, J.; Cool, T. A.; Yang, B.; Yang, R.; Wei, L. X.; Huang, C. Q.; Wang, J.; Qi, F.; Law, M. E.; Westmoreland, P. R. *J. Phys. Chem. A* **2006**, *110*, 3670.

(19) Hansen, N.; Klippenstein, S. J.; Miller, J. A.; Wang, J.; Cool, T. A.; Law, M. E.; Westmoreland, P. R.; Kasper, T.; Kohse-Hoinghaus, K. *J. Phys. Chem. A* **2006**, *110*, 4376.

(20) Hansen, N.; Kasper, T.; Klippenstein, S. J.; Westmoreland, P. R.; Law, M. E.; Kohse-Hoinghaus, K.; Taatjes, C. A.; Wang, J.; Cool, T. A. *J. Phys. Chem. A* **2007**, *111*, http://dx.doi.org/10.1021/jp0683317.

(21) Bhargava, A.; Westmoreland, P. R. *Combust. Flame* **1998**, *113*, 333.

(22) Klippenstein, S. J.; Harding, L. B.; Georgievskii, Y. *Proc. Combust. Inst.* **2007**, *31*, 221−229.

(23) Dunning, T. H., Jr. *J. Chem. Phys.* **1989**, *90*, 1007.

(24) Kendall, R. A., Dunning, T. H., Jr.; Harrison, R. J. *J. Chem. Phys.* **1992**, *96*, 6796.

(25) Woon, D. E., Dunning, T. H., Jr. *J. Chem. Phys.* **1993**, *98*, 1358.

(26) Celani, P.; Werner, H.-J. *J. Chem. Phys.* **2000**, *112*, 5546.

(27) MOLPRO is a package of ab initio programs written by Werner, H.-J. and Knowles, P. J. with contributions from Almlof, J., Amos, R. D., Berning, A., Cooper, D. L., Deegan, M. J. O., Dobbyn, A. J., Eckert, F., Elbert, S. T., Hampel, C., Lindh, R., Lloyd, A. W., Meyer, W., Nicklass, A., Peterson, K., Pitzer, R., Stone, A. J., Taylor, P. R., Mura, M. E., Pulay, P., Schutz, M., Stoll, H., Thorsteinsson, T. The majority of calculations reported here were done with Version 2002.6.

(28) Werner, H.-J.; Knowles, P. J. *J. Chem. Phys.* **1985**, 82, 5053; Knowles, P. J.; Werner, H.-J. *Chem. Phys. Lett.* **1985**, *115*, 259.

(29) Frisch, M. J.; Trucks, G. W.; Schlegel, H. B.; Scuseria, G. E.; Robb, M. A.; Cheeseman, J. R.; Zakrzewski, V. G.; Montgomery, J. A., Jr.; Stratmann, R. E.; Burant, J. C.; Dapprich, S.; Millam, J. M.; Daniels, A. D.; Kudin, K. N.; Strain, M. C.; Farkas, O.; Tomasi, J.; Barone, V.; Cossi, M.; Cammi, R.; Mennucci, B.; Pomelli, C.; Adamo, C.; Clifford, S.; Ochterski, J.; Petersson, G. A.; Ayala, P. Y.; Cui, Q.; Morokuma, K.; Malick, D. K.; Rabuck, A. D.; Raghavachari, K.; Foresman, J. B.; Cioslowski, J.; Ortiz, J. V.; Stefanov, B. B.; Liu, G.; Liashenko, A.; Piskorz, P.; Komaromi, I.; Gomperts, R.; Martin, R. L.; Fox, D. J.; Keith, T.; Al-Laham, M. A.; Peng, C. Y.; Nanayakkara, A.; Gonzalez, C.; Challacombe, M.; Gill, P. M. W.; Johnson, B. G.; Chen, W.; Wong, M. W.; Andres, J. L.; Head-Gordon, M.; Replogle, E. S.; Pople, J. A. *Gaussian 98*; Gaussian, Inc.: Pittsburgh, PA, 1998.

(30) Michael, J. V.; Su, M.-C.; Sutherland, J. W.; Harding, L. B.; Wagner, A. F. *J. Phys Chem A* **2003**, *107*, 10533.

(31) Michael, J. V.; Su, M.-C.; Sutherland, J. W.; Harding, L. B.; Wagner, A. F. *Proc. Combust. Inst.* **2005**, *30*, 965.

(32) Miller, J. A.; Klippenstein, S. J. *Phys. Chem. Chem. Phys.* **2004**, *6*, 1192.

(33) Hanning-Lee, M. A.; Pilling, M. J. *Int. J. Chem. Kinet.* **1992**, *24*, 271.

(34) Atkinson, D. B.; Hudgens, J. W. *J. Phys. Chem. A* **1999**, *103*, 4242.

(35) Wheeler, S. E.; Allen, W. D.; Schaefer, H. F. *J. Chem. Phys.* **2004**, *121*, 8800.

(36) Wang, H.; Brezinsky, K. *J. Phys. Chem. A* **1998**, *102*, 1530.

(37) Emdee, J. L.; Brezinsky, K.; Glassman, I. *J. Phys. Chem.* **1992**, *96*, 2151.

(38) Frank, P.; Herzler, J.; Just, T.; Wahl, C. *Proc. Combust. Inst.* **1994**, *25*, 833.

(39) Roy, K.; Braun-Unkhoff, M.; Frank, P.; Just, T. *Int. J. Chem. Kinet.* **2001**, *33*, 821; **2002**, *34*, 209.

(40) Dean, A. M. *J. Phys. Chem.* **1990**, *94*, 1432.

(41) Zhong, X.; Bozzelli, J. W. *J. Phys. Chem. A* **1998**, *102*, 3537.

(42) Tokmakov, I. V.; Moskaleva, L. V.; Lin, M. C. *Int. J. Chem. Kinet.* **2004**, *36*, 139.

(43) Bartels, M.; Edelbuttel-Einhaus, J.; Hoyermann, K. *Proc. Combust. Inst.* **1989**, *22*, 1041.

(44) Ackerman, L.; Hippler, H.; Pagsberg, P.; Reihs, C.; Troe, J. *J. Phys. Chem.* **1990**, *94*, 5247.